ORIGINAL ARTICLE

Discovery of WS-157 as a highly potent, selective and orally active EGFR inhibitor

Pengxing He[a,†], Shenghui Niu[a,†], Shuai Wang[a,†], Xiaojing Shi[a],
Siqi Feng[a], Linna Du[a], Xuyang Zhang[a], Zhilu Ma[a], Bin Yu[a,b,*],
Hongmin Liu[a,*]

[a]School of Pharmaceutical Sciences, Zhengzhou University, Zhengzhou 450001, China
[b]State Key Laboratory of Pharmaceutical Biotechnology, Nanjing University, Nanjing 210023, China

Abstract   EGFR tyrosine kinase inhibitor (EGFR-TKI) has been used successfully in clinic for the treatment of solid tumors. In the present study, we reported the discovery of **WS-157** from our in-house diverse compound library, which was validated to be a potent and selective EGFR-TKI. **WS-157** showed excellent inhibitory activities against EGFR (IC_{50} = 0.81 nmol/L), EGFR[d746−750] (IC_{50} = 1.2 nmol/L) and EGFR[L858R] (IC_{50} = 1.1 nmol/L), but was less effective or even inactive against other nine kinases. **WS-157** also displayed excellent antiproliferative activities against a panel of human cancer cell lines, and exhibited the ability to reduce colony formation and wound healing the same as gefitinib. We found that **WS-157** upon oral administration showed better anti-tumor activity in A431 bearing xenograft mouse models compared to gefitinib. In addition, **WS-157** showed better intestinal absorption than gefitinib and had favorable pharmacokinetic properties and microsomal metabolic stability in different species. These studies indicate that **WS-157** has strong antitumor activity *in vitro* and *in vivo*, and could be used for the development of anti-lung cancer agent targeting EGFR.

---

*Corresponding authors.

   E-mail addresses: yubin@zzu.edu.cn (Bin Yu), liuhm@zzu.edu.cn (Hongmin Liu).

†These authors made equal contributions to this work.

1. Introduction

The human epidermal growth factor receptor (EGFR) belongs to the ErbB family of receptor tyrosine kinases consisting of four members (ErbB1–4). All ErbB family members share a common structure organization that is composed of an extracellular ligand binding domain, a transmembrane domain, and an intracellular domain with tyrosine kinase activity[1]. The binding of their respective ligands to the corresponding ErbB extracellular domains induces homodimerization or heterodimerization of the receptors and subsequent phosphorylation at the multiple tyrosine residues located in the intracellular region, and then phosphorylated tyrosine residues recruit diverse effector proteins to activate multiple signal transduction pathways, including the mitogen-activated protein kinase (MAPK) pathway and the phosphatidylinositol 3-kinase (PI3K)/AKT pathway[2–4]. Aberrant EGFR activation promotes multiple biological processes, including survival, proliferation, invasion, metastasis, angiogenesis and decreased apoptosis, which play central roles in the progression of tumors[1].

Blocking or inhibiting signaling pathways with EGFR tyrosine kinase inhibitor (EGFR-TKI) has resulted in development of several novel EGFR-TKI (Fig. 1)[5–8]. The first generation of EGFR-TKI, including gefitinib[9], erlotinib[10], and icotinib[11], are ATP competitive reversible inhibitors for the treatment of non-small-cell lung cancer (NSCLC). Although gefitinib and erlotinib are effective in the treatment of NSCLC, especially in patients with tumors possessing EGFR-sensitive mutants (EGFR[L858R]), its resistance has been observed clinically and was associated with the T790M mutation of EGFR[12,13]. The second generation EGFR-TKIs, such as afatinib/BIBW2992[14,15] and lapatinib, are irreversible inhibitors. Afatinib was approved by FDA in July 2013 for first-line treatment of subjects with EGFR exon 19 deletions or exon 21 (L858R) substitution mutations[16]. Osimertinib, rociletinib and olmutinib are the newly developed "third-generation" EGFR-TKIs that efficiently overcome the EGFR[T790M] drug-resistance mutation while sparing the EGFR wt. Rociletinib and osimertinib exhibited excellent clinical efficacy in NSCLC patients harboring EGFR[T790M] with more than 50% response rates and

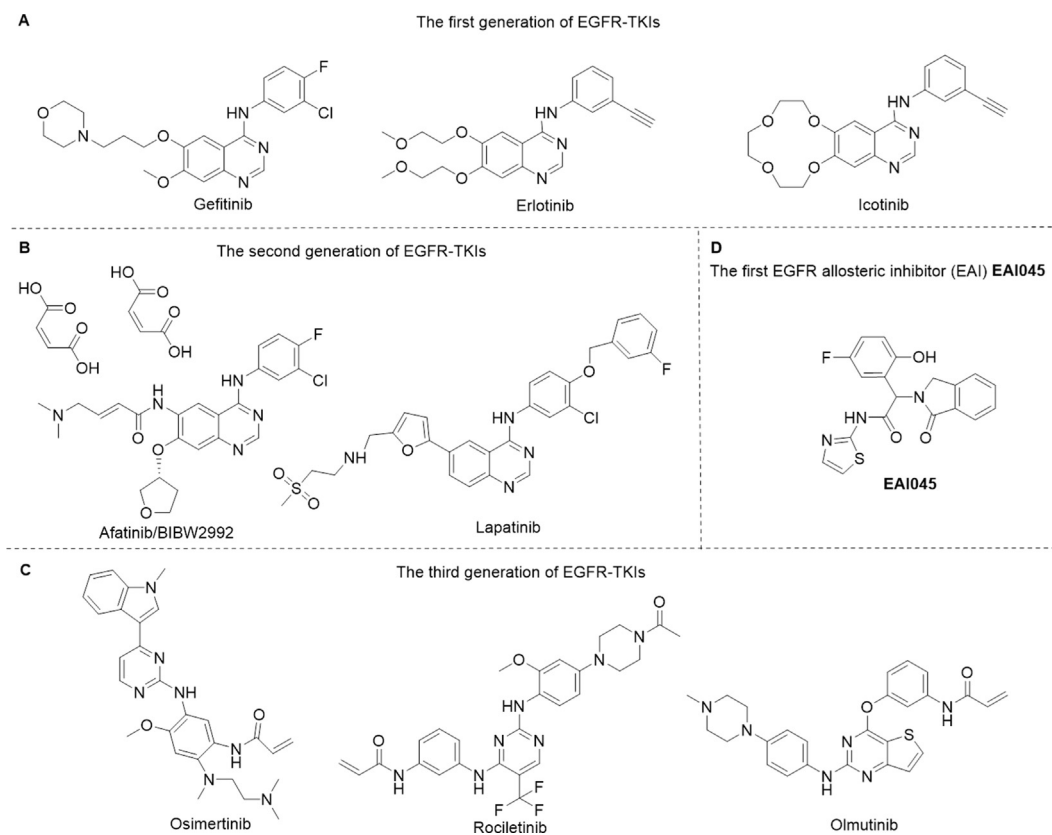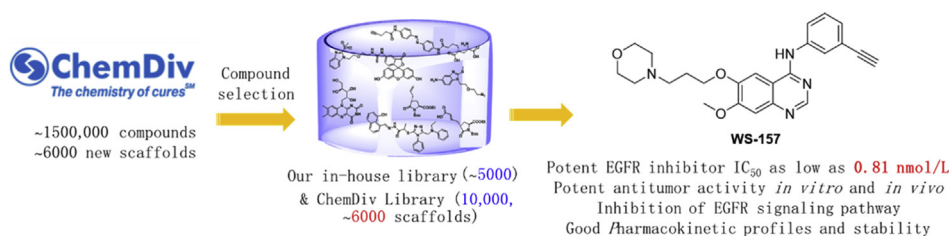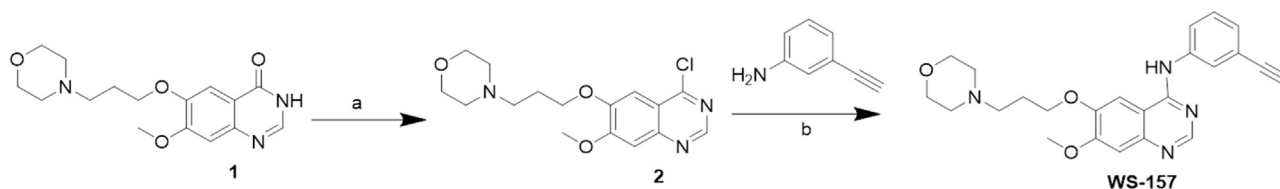**Figure 1**   Representative EGFR inhibitors.

Figure 2   Discovery of **WS-157** as a potent EGFR inhibitor. **WS-157** was identified from our combined diverse compound library based on the random screening against EGFR tyrosine kinase.

Scheme 1 Synthesis of **WS-157**. Reagents and conditions: (a) POCl$_3$, 90 °C, 5−6 h, reflux; (b) EtOH, TEA, r.t., 3 h.

less skin and gastrointestinal toxicities than those typically observed for the first generation EGFR TKIs[17,18].

Recently, osimertinib was approved by FDA for the treatment of patients with metastatic EGFR[T790M] mutation positive NSCLC who have progressed on or after EGFR TKI therapy[19]. Unfortunately, resistance to third-generation EGFR inhibitors may occur during treatment and C797S has been shown to be an acquired drug resistance mutation in NSCLC patients with EGFR[T790M] mutation[16,20]. Therefore, it is highly needed for the development of new drugs that overcome EGFR mutations. Recently, the first EGFR allosteric inhibitor (EAI) **EAI045** was reported. This compound, in combination with the antibody cetuximab, inhibits EGFR[L858R/T790M] and EGFR[L858 R/T790M/C797S] *in vitro* and in animal models[21].

First generation inhibitors, such as gefitinib and erlotinib, have been used in clinical treatment of NSCLC for many years. However, their limited therapeutic spectrum against cancer and inevitable acquired drug resistance require continuous efforts in developing new EGFR inhibitors. Here, we report the discovery of new EGFR inhibitor **WS-157** from our in-house compound collection (∼15,000 compounds, ∼6000 scaffolds), anticancer evaluation, and early preclinical evaluation as a new orally available EGFR inhibitor with strong antitumor activity (Fig. 2). **WS-157** effectively inhibited EGFR phosphorylation and downstream signal transduction, and has a significant inhibitory effect on tumor growth *in vivo* and *in vitro*.

2. Results

2.1. Synthesis of WS-157

As shown in Scheme 1, the synthesis of **WS-157** started from commercially available compound **1**; chlorination of compound **1** in POCl$_3$ gave compound **2**, which then reacted with 3-ethynylaniline to form **WS-157** in the presence of TEA.

2.2. WS-157 potently and selectively inhibits EGFR kinase activity in vitro

In order to determine the selectivity profile of **WS-157**, the effects of **WS-157** on the enzymatic activity of a panel of 16 tyrosine kinases consisting of EGFR, EGFR[d746−750], EGFR[L858R], EGFR[T790M/L858R], EGFR[T790M], FGFR1, HER4, KDR (VEGFR2), PDGFRα (PDGFRA), PDGFRβ (PDGFRB), IGF1R, SRC, FLT1, MET, KIT and HER2 were examined. Gefitinib was chosen as reference drug (Table 2). The results indicated that **WS-157** showed excellent inhibitory activities against EGFR (IC$_{50}$ = 0.81 nmol/L), EGFR[d746−750] (IC$_{50}$ = 1.2 nmol/L) and EGFR[L858R] (IC$_{50}$ = 1.1 nmol/L), which was more potent than gefitinib. In addition, the IC$_{50}$ values of this compound against HER4, HER2, EGFR[T790M/L858R] and EGFR[T790M] were 12, 90,

Table 1 Kinases and control compounds.

Kinase	Manufacturer	Item number	Lot number
EGFR	Carna	08−115	13CBS-0005X
EGFR[d746−750]	Carna	08−527	11CBS-1129H
EGFR[L858R]	Carna	08−502	13CBS-0537F
EGFR[T790M/L858R]	Carna	08−510	12CBS-0765H
EGFR[T790M]	Carna	08−194	08CBS-0510N
FGFR1	Carna	08−133	12CBS-0123K
HER4	Carna	08−118	08CBS-0652J
KDR (VEGFR2)	Carna	08−191	13CBS-0442H
PDGFRα (PDGFRA)	Carna	08−156	11CBS-1067P
PDGFRβ (PDGFRB)	Carna	08−157	09CBS-1164P
IGF1R	Carna	08−158	12CBS-0573J
SRC	Carna	08−016	15CBS-0769C
FLT1	Carna	08−141	09CBS-0414H
MET	Carna	08−189	09CBS-0092J
KIT	Carna	08−151	10CBS-1118P
HER2	Carna	08−173	10CBS-1134K
Afatinib	Selleckchem	S1011	lot10
AZD9291	Selleckchem	S7297	lot07
BGJ398	Selleckchem	S2183	NVP-BGJ398
Nintedanib	Selleckchem	S1010	S101004
Saracatinib	Selleckchem	S1006	lot03
Staurosporine	Selleckchem	S1421	S142105
DMSO	Sigma	D8418-1L	SHBG3288V

230 and 348 nmol/L respectively, which were similar to those of gefitinib. For the other nine kinases, **WS-157** had low or no inhibitory activity with the IC$_{50}$ values more than 1000 nmol/L. The result indicates that **WS-157** is a highly selective inhibitor

Table 2 Differential inhibitory activities of **WS-157** and gefitinib against a panel of tyrosine kinases.

Kinase	WS-157 (nmol/L)	Gefitinib (nmol/L)
EGFR	0.81±0.01	0.96
EGFR[d746−750]	1.23±0.03	1.43±0.04
EGFR[L858R]	1.05±0.01	1.268±0.02
EGFR[T790M/L858R]	208.9±0.57	296.4±0.99
EGFR[T790M]	344.05±20.72	70.56±1.28
FGFR1	>10,000	>10,000
HER4	10.98±0.78	10.55±0.17
KDR (VEGFR2)	4384.50±135.06	5465.5±122.33
PDGFRα (PDGFRA)	3446.50±210.01	2040±77.78
PDGFRβ (PDGFRB)	1180±113.40	1506±2.83
IGF1R	>10,000	>10,000
SRC	5210±386.08	3403.5±17.68
FLT1	5020.50±153.44	>10,000
MET	>10,000	9725±961.67
KIT	>10,000	>10,000
HER2	90.82±12.45	78.03±1.78

that targets EGFR family members, particularly EGFR, EGFR[d746−750] and EGFR[L858R].

2.3. WS-157 suppresses the biochemical pathways in human EGFR wt cell lines

The PI3K/AKT pathways are the downstream signaling transduction of EGFR and is critical for tumor proliferation, survival and response to exterior stimuli[25]. We next tested the ability of WS-157 to inhibit the phosphorylation of EGFR and its downstream AKT in human A431 cell, with gefitinib as a reference drug. As shown in Fig. 3A, exposure of cells to the growth factor

EGF rapidly increased the level of cellular p-EGFR and p-AKT, but WS-157 could dramatically and dose-dependently inhibit EGF-induced p-EGFR and p-AKT similar to gefitinib. Moreover, 1.0 μmol/L of WS-157 or gefitinib almost completely prevented the p-EGFR and p-AKT stimulated by EGF (Fig. 3A). Similar results were obtained for additional EGFR wt cell lines of other cancer types, including NSCLC and gastric cancer (Fig. 3B−F). Then, we detected the effect of WS-157 in EGFR[T790M/L858R] cell line NCI−H1975 and found that WS-157 and gefitinib did not prevent p-EGFR and p-AKT (Fig. 3G), which indicated that WS-157 was an EGFR wt inhibitor. As gefitinib is a well-known first generation reversible EGFR inhibitor, we also explored whether
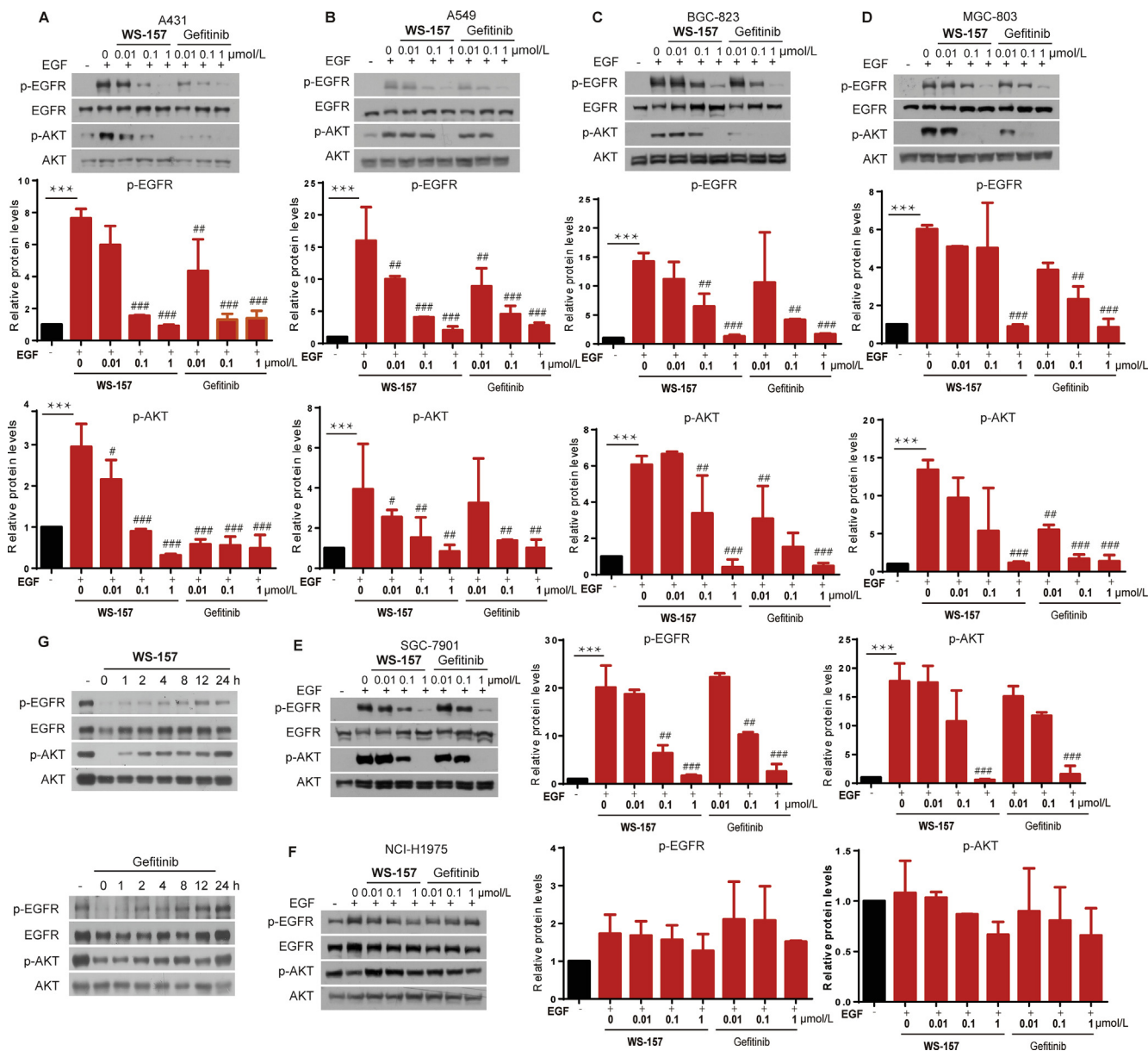

Figure 3 WS-157 suppressed the biochemical pathways in different cell lines. (A) A431 cells, (B) A549 cells, (C) BGC-823 cells, (D) MGC-803 cells, (E) SGC-7901 cells and (F) NCI−H1975 cells were starved for 24 h, treated with increasing concentrations of WS-157 or gefitinib for 1 h, and exposed to EGF (50 ng/mL) for 10 min. (G) A549 cells were treated with WS-157 or gefitinib for 2 h and incubated for 0−24 h after removal of WS-157 or gefitinib. The cell lysates were collected for Western blotting with the indicated antibodies. The representative data of at least three independent experiments are shown, $^{*}P < 0.05$, $^{**}P < 0.01$, $^{***}P < 0.001$, normal control vs. EGF-stimulated control (mean ± SD, $n = 3$); $^{\#}P < 0.05$; $^{\#\#}P < 0.01$; $^{\#\#\#}P < 0.001$ vs. EGF-stimulated control (mean ± SD, $n = 3$).

inhibitory activities of **WS-157** was reversible. Cells were washed to remove the unbounded compounds after treatment with **WS-157** for 2 h and incubated in fresh medium 0−24 h. The results indicated that inhibition of p-EGFR and p-AKT were gradually recovered after removal of **WS-157**. All these data suggest that **WS-157** is a highly selective and reversibly EGFR inhibitor.

2.4. Effects of WS-157 on tumor cell proliferation, clone assay and migration

Having established that **WS-157** can selectively inhibit EGFR, we investigated the effects of **WS-157** on tumor cell proliferation, clone assay and migration. SRB assays was used to examine the proliferative inhibition of **WS-157** on 12 tumor cell lines that possess distinct levels of EGFR protein, with gefitinib as a reference drug (Fig. 4). As shown in Fig. 4A, **WS-157** showed varied antiproliferative activities against the tested tumor cells, and for most of the cells, the IC_{50} values of **WS-157** were similar to those of gefitinib. Particularly, **WS-157** remarkably inhibited the proliferation of PC-9 and A431 cells with the IC_{50} values less than 1.0 μmol/L (the inhibitory cures of **WS-157** against PC-9, A431 and GES-1 have been provided in Supporting Information Fig. S1). As shown in Fig. 4B−D, the results suggest that **WS-157** had excellent inhibitory activities on cell proliferation and migration. Particularly, **WS-157** almost completely inhibited proliferation and migration of PC-9 at 0.1 μmol/L.

2.5. WS-157 inhibits growth of A431 human tumor xenografts

Given its encouraging *in vitro* antitumor activity, we examined the antitumor efficacy of **WS-157** in xenograft mouse models of A431 overexpressing EGFR wt. According to the reported data, oral administration of gefitinib (10 mg/kg body weight once daily) could induce tumor regression, while **WS-157** (10 mg/kg/day) showed slightly better anti-tumor activity compared to gefitinib (Fig. 5A and B). However, the tumor burden in nude mice was nearly completely suppressed by **WS-157** (40 mg/kg/day) (Fig. 5A−C). Meanwhile, body weights of nude mice measured concurrently showed no obvious differences during the treatment, demonstrating that **WS-157** was well tolerated (Fig. 5D). We also examined the effect of **WS-157** on the EGFR signaling pathway in tumor extracts. As shown in Fig. 5E and F, p-EGFR and p-AKT were clearly inhibited by **WS-157** or gefitinib.

2.6. Caco-2 cell permeability

Caco-2 cell monolayer has become a commonly used *in vitro* model for intestinal absorption of drugs[26]. As shown in Table 3, the P_{app} (A−B) value of metoprolol was 40.04, and it was used as a high permeable control. On the contrary, the P_{app} (A−B) value of atenolol was 0.66, which was considered as a low permeable control. The P_{app} (B−A)/P_{app} (A−B) value of erythromycin was 240.3, which indicated that more erythromycin was transported from BL to AP. Therefore, erythromycin was used as an efflux
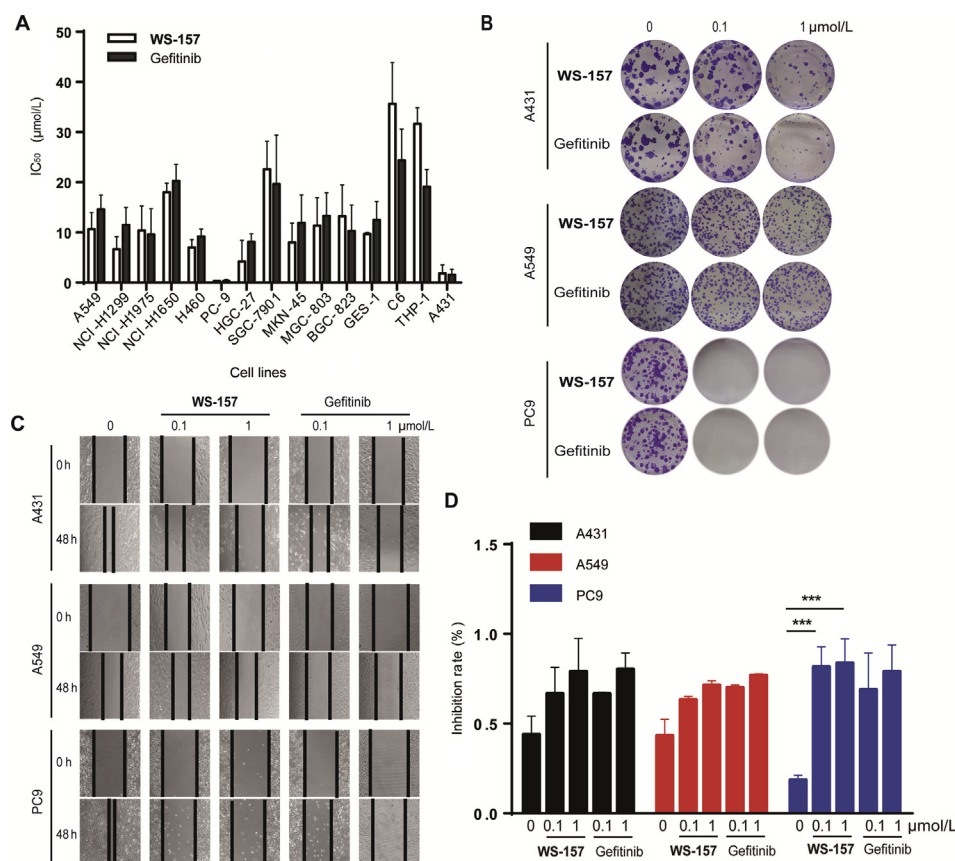
Figure 4 **WS-157** against proliferation, colony formation and wound healing. (A) Cells were treated with **WS-157** or gefitinib for 72 h and cell proliferation were measured by sulforhodamine B. (B) 500 Cells or 1000 cells were treated with **WS-157** or gefitinib to form colony for 14 days. (C) and (D) Scratched cells continued to grow for 48 h. Graph shows the inhibition rate (%) of cell migration, $^*P < 0.05$, $^{**}P < 0.01$, $^{***}P < 0.001$ compared with control group (mean ± SD, $n = 3$). The representative data are shown.

Figure 5 *In vivo* antitumor effects of compound **WS-157**. Effect of **WS-157** (10, 40 mg/kg/d) or gefitinib (10 mg/kg/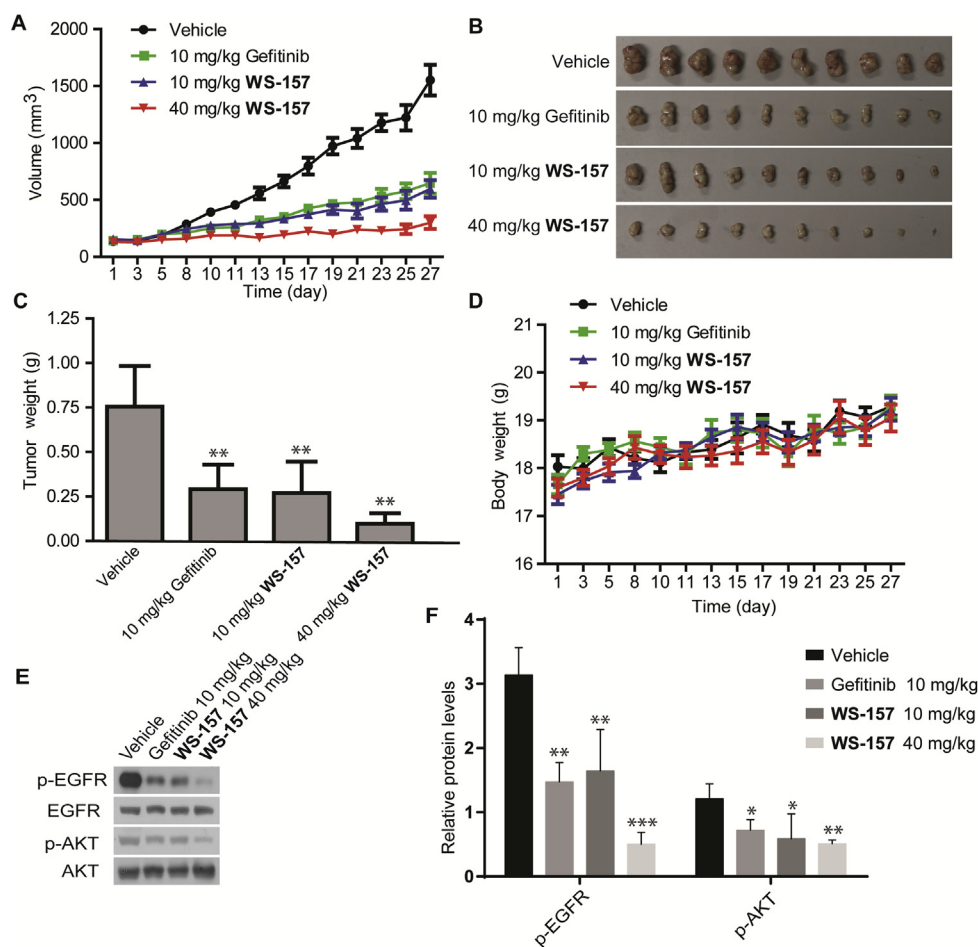d) on growth of A431 human tumor xenografts for 28 days. (A) Tumor volume during the administration period. (B) Tumor sizes. (C) Tumor weight. (D) Body weight of mice. (E) and (F) The tumor tissue protein was extracted and p-EGFR and p-AKT was detected by Western blot. The data shown represent the mean $\pm$ SD. $^{**}P < 0.01$, $^{***}P < 0.01$ (mean $\pm$ SD, $n = 3$).

substrate. The P_{app} (A–B) values of **WS-157** and gefitinib were 9.13 and 8.37, respectively. The P_{app} (B–A)/P_{app} (A–B) values of **WS-157** and gefitinib were 2.51 and 1.85, respectively.

2.7. Metabolic stability

WS-157 was incubated individually with different species to assess the metabolic stability of interspecies difference. We further

compared the different metabolism between **WS-157** and gefitinib in liver microsome in this study. As shown in Fig. 6, both **WS-157** and gefitinib were the most stable in the dog liver microsome, followed by human, rat, mouse and monkey. It was indicated that the metabolic stability of **WS-157** and gefitinib was similar, except in rat. The $t_{1/2}$ of **WS-157** and gefitinib in rat liver microsome was 11.78 and 21.16, respectively, which indicated that **WS-157** was less stable than gefitinib in rat liver microsome (Table 4).

2.8. Pharmacokinetic study

In order to investigate the pharmacokinetic characteristics of **WS-157**, we determined the plasma concentration of **WS-157** in rats after intravenous injection (i.v.) or *p.o.* administration. Gefitinib was used as a control. As shown in Fig. 7, the mean plasma concentration−time curves of **WS-157** and gefitinib groups were similar after i.v. administration. Based on non-compartment model analysis, the pharmacokinetic parameters were calculated and summarized in Table 5. Parameters, such as CL, $t_{1/2}$ and AUC were analogous between **WS-157** and gefitinib after i.v. treatment, but mean residence time (MRT) of **WS-157** was shorter than that of gefitinib. In this study, the C_{max} of **WS-157** was slightly higher and earlier than that of gefitinib, which was consistent with the

Table 3 Permeability coefficients of the compounds.

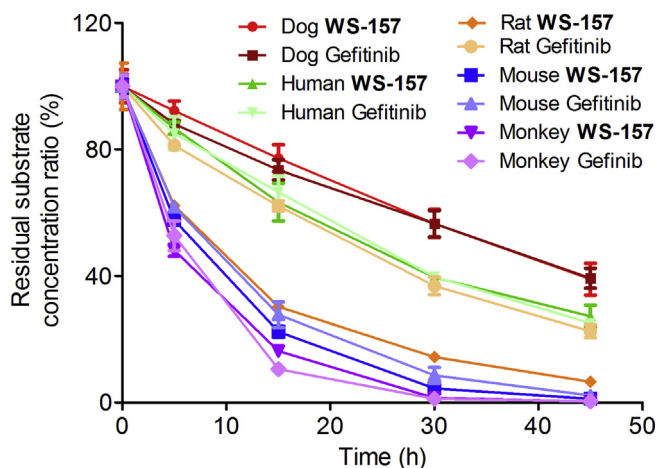| Test article	Direction	P_{app} $(10^{-6}$ cm/s) Mean $\pm$ RSD	P_{app} (B–A)/ P_{app} (A–B)
Metoprolol	A–B	40.04 ± 0.05	0.77
	B–A	30.92 ± 0.03	
Atenolol	A–B	0.66 ± 0.01	2.31
	B–A	1.53 ± 0.01	
Erythromycin	A–B	0.09 ± 0.03	240.3
	B–A	22.18 ± 0.02	
WS-157	A–B	9.13 ± 0.02	2.51
	B–A	22.91 ± 0.02	
Gefitinib	A–B	8.37 ± 0.01	1.85
	B–A	15.52 ± 0.02	

Figure 6 Metabolic stability. Metabolic stability of the **WS-157** (1 μmol/L) and gefitinib (1 μmol/L) in liver microsomes of human, rat, mouse, dog and monkey. The results are expressed as the % of remaining substrate concentration ratio of the compounds after different time of incubation.

Table 4 The $t_{1/2}$ of **WS-157** and gefitinib in liver microsomes of different species.

Species	$t_{1/2}$ (min)	
	WS-157	Gefitinib
Human	23.64	22.51
Rat	11.78	21.16
Mouse	7.01	8.38
Dog	33.24	34.48
Monkey	5.01	4.66

better intestinal absorption of **WS-157** in Caco-2 cell permeability assay. The oral bioavailability of **WS-157** and gefitinib were 86.2 ± 19.7% and 66.5 ± 22.8%, respectively, which had no statistically significant difference.

3. Discussion

EGFR has emerged as a key target for anticancer therapeutics. Tyrosine kinase inhibitors, such as erlotinib, gefitinib, icotinib, and lapatinib, are recommended as first-line treatments for NSCLC patients. By screening our diverse compound collection against EGFR[27−29], we identified some promising hit compounds, of which **WS-157** was fully characterized as a potent and selective EGFR-TKI with excellent potency *in vivo* and *in vitro*. Compared with gefitinib, **WS-157** showed better inhibitory activities against EGFR, EGFR[d746−750] and EGFR[L858R], but was less potent against EGFR[T790M]. This was further confirmed by the effects of **WS-157** on the biochemical pathways in cells. EGFR is stimulated by a number of autocrine growth factors, including EGF and PI3K/AKT is one of major downstream effectors following EGFR activation[25]. **WS-157** dose-dependently inhibited EGF-induced p-EGFR and p-AKT in EGFR wt cells, but was ineffective in EGFR[T790M/L858R] mutation NCI−H1975 cells. We also explored the inhibitory effect of **WS-157** on EGFR, showing that the inhibition of **WS-157** on EGFR activation was gradually recovered after the removal of **WS-157**, and the activity was completely recovered after 12 h. Thus, our findings suggest that **WS-157** is a selective and reversible EGFR TKI.

WS-157 displayed excellent antiproliferative activities against a panel of human cancer cell lines and the IC$_{50}$ values of this compound were similar to those of gefitinib. Particularly, **WS-157** significantly inhibited the proliferation of PC-9 and A431 cells (IC$_{50}$ < 1.0 μmol/L). In addition, **WS-157** had excellent inhibitory activities on cell proliferation and migration. Furthermore, the *in vivo* antitumor activity of **WS-157** was also carried out in xenograft models bearing A431 cells, a recognized model for the testing of biological effects on EGFR signaling[30]. **WS-157** inhibited the growth of A431 xenografts in a dose-dependent manner, and complete inhibition was observed in animals receiving a daily i.g. doses of 40 mg/kg **WS-157**. Interestingly, we observed that **WS-157** showed slightly better anti-tumor activity compared to gefitinib at the same dose (10 mg/kg/day). However, weight loss observed during the administration of **WS-157** was not influenced. Therefore, our data demonstrate that **WS-157** exhibits promising antitumor activity and the slightly greater weight losses observed in the present study might reflect the greater duration of dosing and more chemo-sensitive nature of the nude mice used.

In our study, the P_{app} (A−B) value of **WS-157** was higher than that of gefitinib, which indicated that the intestinal absorption of **WS-157** was better than that of gefitinib. In addition, the P_{app} (B−A)/P_{app} (A−B) values of **WS-157** and gefitinib were both higher than 1.5, suggesting that **WS-157** and gefitinib might be the substrates of the efflux transporters. Several receptor kinase inhibitors were found to interact with the ATP binding site of major ABC transporters, including gefitinib, vandetanib, pelitinib and
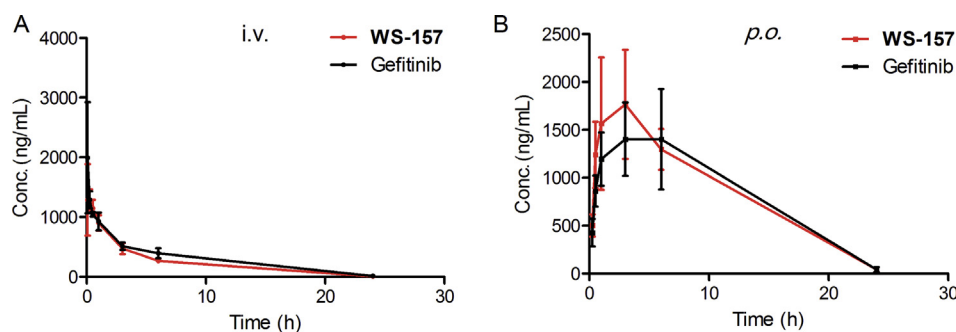

Figure 7 Mean plasma concentration−time profile. (A) **WS-157** and gefitinib after i.v. administration of 10 mg/kg, respectively (mean ± SD, n = 3). (B) **WS-157** and gefitinib after *p.o.* administration of 40 mg/kg, respectively (mean ± SD, n = 3).

Table 5 The main pharmacokinetic parameters of **WS-157** and Gefitinib after i.v. (10 mg/kg) and *p.o.* (40 mg/kg) administration (mean $\pm$ SD, $n = 3$).

PK parameter	i.v.		PK parameter	*p.o.*	
	WS-157	Gefitinib		**WS-157**	Gefitinib
CL (L/hr/kg)	1.65 ± 0.23	1.31 ± 0.26	T_{max} (h)	2.33 ± 1.15	4.33 ± 2.89
V_{ss} (L/kg)	6.52 ± 0.91	5.93 ± 0.90	C_{max} (ng/mL)	1799 ± 612	1480 ± 395
$t_{1/2}$ (h)	3.39 ± 0.22	3.85 ± 0.25	$t_{1/2}$ (h)	3.73 ± 0.50	3.85 ± 0.35
AUC_{last_plasma} (h·ng/mL)	6112 ± 896	7722 ± 1426	AUC_{last_plasma} (h·ng/mL)	$20{,}938 \pm 4695$	$20{,}510 \pm 6945$
AUC_{INF_plasma} (h·ng/mL)	6146 ± 908	7803 ± 1462	AUC_{INF_plasma} (h·ng/mL)	$21{,}183 \pm 4832$	$20{,}754 \pm 7102$
MRT_{INF} (h)	3.96 ± 0.24	$4.54 \pm 0.19^{*}$	F (%)	86.2 ± 19.7	66.5 ± 22.8

$^{*}P < 0.05$, gefitinib *vs.* **WS-157**.

neratinib[31−35]. **WS-157** was speculated to modulate the function of ABC transporters.

It was indicated that the metabolic stability of **WS-157** and gefitinib was similar in liver microsome of human, mouse, dog and monkey in our study. However, **WS-157** was less stable than gefitinib in rat liver microsome. To further investigate the pharmacokinetics of gefitinib and **WS-157** *in vivo*, we determined the concentration of **WS-157** and gefitinib in plasma of rats after treatment. For intravenous administration, the pharmacokinetic features of **WS-157** and gefitinib were similar. However, for oral administration, **WS-157** was well absorbed and showed good oral bioavailability ($F = 86.2 \pm 19.7$%), and there was a tendency of increase of the values of C_{max}, AUC, and F in **WS-157** group compared with gefitinib. The higher C_{max} and earlier T_{max} in **WS-157** treatment group suggested better absorption than gefitinib, which is in accordance with the Caco-2 cell permeability assay. These data indicated that **WS-157** had a favorable pharmacokinetic property and deserved further investigation.

4. Conclusions

In summary, **WS-157** was identified from our in-house diverse compound library, which was validated to be a highly potent and selective EGFR-TKI. **WS-157** showed excellent inhibitory activity against EGFR ($IC_{50} = 0.81$ nmol/L), EGFR[d746−750] ($IC_{50} = 1.2$ nmol/L) and EGFR[L858R] ($IC_{50} = 1.1$ nmol/L) and possessed high selectivity over other nine kinases. **WS-157** displayed excellent antiproliferative activities against several human cancer cell lines, and exhibited comparable capability of reducing colony formation and wound healing with gefitinib. We found that **WS-157** upon oral administration showed better anti-tumor activity in A431 bearing xenograft mouse models compared to gefitinib. In addition, **WS-157** showed better intestinal absorption than gefitinib and had favorable pharmacokinetic properties. These studies indicated that **WS-157** had strong antitumor activity *in vitro* and *in vivo*, and could be used for the development of anti-lung cancer agent targeting EGFR.

5. Experimental

5.1. Chemicals and antibodies

Getifinib were purchased from Selleck (Shanghai, China). The HPLC purity of **WS-157** was >98%. All of the above compounds were dissolved in DMSO at 10 mmol/L (used *in vitro*) as a stock solution and stored at −20 °C. RIPA were purchased from Beyotime (Nantong, China). EGFR (Cell Signaling Technology, 4223S, Boston, USA), p-EGFR (Cell Signaling Technology,

2772S), AKT (Cell Signaling Technology, 4223S), p-AKT (Cell Signaling Technology, 9728S) and anti-GAPDH antibody were purchased from Cell Signaling Technology. HRP-conjugated donkey anti-goat IgG was obtained from The Golden Bridge.

5.2. The synthetic routes for the synthesis of compound WS-157

Compound 1 (1g, 3.13 mmol) was dissolved in POCl$_3$ (10 mL), which was then stirred at 90 °C for 5−6 h. The mixture was subjected to evaporation of the solvent to generate the unstable compound 2. Compound 2 (200 mg, 592.06 μmol) then reacted with 3-ethynylaniline (69.36 mg, 592.06 μmol) in the presence of triethylamine (179.74 mg, 1.78 mmol) in ethanol at room temperature for 3 h, generating the target compound **WS-157**. White solid, yield: 84%. ^{1}H NMR (400 MHz, DMSO-d_6) δ 11.18 (s, 1H), 8.86 (s, 1H), 8.64 (s, 1H), 7.93 (s, 1H), 7.85 (d, $J = 8.1$ Hz, 1H), 7.49 (t, $J = 8.1$ Hz, 1H), 7.43 (s, 1H), 7.40 (d, $J = 7.7$ Hz, 1H), 4.39 (t, $J = 6.0$ Hz, 2H), 4.29 (s, 1H), 3.98 (m, 5H, overlapped), 3.85 (t, $J = 11.8$ Hz, 2H), 3.50 (d, $J = 11.8$ Hz, 2H), 3.37−3.25 (m, 2H), 3.18−3.03 (m, 2H), 2.35 (m, 2H). ^{13}C NMR (100 MHz, DMSO-d_6) δ 158.13, 156.31, 148.93, 148.68, 137.33, 135.77, 129.21, 129.01, 127.59, 125.34, 121.90, 107.33, 105.62, 99.88, 82.97, 81.25, 67.31, 63.18, 56.50, 53.50, 51.11, 22.74. HR-MS (ESI): m/z Calcd. for $C_{24}H_{27}N_4O_3$ [M+H]$^+$, 419.2083; Found 419.2062.

5.3. Kinase inhibition assay

The kinases and control compounds used in the experiments are shown in Table 1. The kinase assays were performed in 384-well plates. In briefly, 10 mmol/L tested compounds was diluted 4 times with DMSO to 10 concentrations. Then, 2.5 nmol/L of the kinase, 3 μmol/L kinase peptide22 (5-FAM-EEPLYWSFPAKKK-CONH$_2$), 80.8 μmol/L of ATP, and 250 nL of **WS-157** or control compounds were added to the reaction buffer (50 mmol/L HEPES, 0.01% Triton X-100, 10 mmol/L MgCl$_2$, 2 mmol/L DTT) to initiate the reaction. After incubate at room temperature for 30 min, the reactions were stopped by adding 25 μL stop buffer (100 mmol/L HEPES, 0.015% Brij-35, 50 mmol/L EDTA). The reaction mixture was analyzed with Caliper EZ Reader (Waltham, MA, USA), and the conversion values were converted to inhibition.

5.4. Cell lines and culture

Human NSCLC NCI−H1975 cell lines were provided by the group of Ding Jian, the Shanghai Institute of Materia Medica, Chinese Academy of Sciences (China). Human NSCLC A549,

NCI−H1650, NCI−H1299, PC9 and H460 cell lines, human gastric adenocarcinoma GES-1, BGC-823, SGC-7901, MGC-803 and MKN-45 cell lines, human squamous cell carcinoma A431 cell lines, human monocytic cell line THP-1, human colon adenocarcinoma Caco-2 cell lines and Rat glioma C6 cell lines were obtained from the cell bank of the Shanghai Institute of Materia Medica, Chinese Academy of Sciences (China). The cells were maintained in RPMI-1640 medium (NCI−H1975, A549, NCI−H1650, NCI−H1299, PC9, H460, BGC-823, SGC-7901 and MKN-45) or Dulbecco's modified essential medium (GES-1, MGC-803 and Caco-2). All cells were supplemented with 10% heat-inactivated fetal calf serum (FBS; Gibco) at 37 °C in a 5% CO_2 humidified environment.

5.5. Cell proliferation assays

WS-157 was examined against a panel of cell lines. Gefitinib was used as a reference compound and was applied in parallel. Cell proliferation was evaluated using the SRB (sulforhodamine B) assay as previously described[22,23]. Briefly, cells plated in 96-well plates were treated with gradient concentrations of compounds at 37 °C for 72 h. Cells were then fixed with 10% trichloroacetic acid (TCA), washed with distilled water, and stained with SRB (Sigma, St. Louis, MO, USA) in 1% acetic acid. SRB in the cells was dissolved in 10 mmol/L Tris−HCl and was measured at 560 nm with a spectraMAX190 (Molecular Devices, Sunnyvale, CA, USA). IC_{50} values were obtained using GraphPad Prism 5 based on the results of at least 3 independent tests.

5.6. Western blotting analyses

Cells were seeded in six-well plates and starved in serum-free medium for 24 h. After exposed to the indicated concentrations of compounds for 1 h, cells were stimulated with 50 ng/mL EGF for 10 min. Treated cells were lysed with RIPA buffer (Solarbio, Beijing, China). Equal amounts of proteins were fractionated by SDS−PAGE and transferred to nitrocellulose membranes (Thermo Scientific, Franklin, MA, USA), which were blocked with 5% (w/v) milk in TBST for 2 h before overnight incubation with primary antibody diluted in 3% (w/v) BSA in TBST. HRP-conjugated secondary antibody (Jackson ImmunoResearch Laboratories, West Baltimore, PA, USA) was applied for 2 h and detected by ECL (Thermo Scientific, USA).

5.7. Colony formation assay

Colony formation assay was performed as described previously[24]. A431 cells (500 cells/well), PC-9 (1000 cells/well) and A549 cells (1000 cells/well) were seeded in a 6-well plate and incubated for 24 h, and then the media was replaced with fresh media containing different concentrations of agents for another 14 days. Then, the cells were washed twice with PBS and fixed with 4% para-formaldehyde for 30 min. Crystal violet staining was used to stain the cell for 30 min at 37 °C. After that, the staining was washed away with PBS until the colonies were clear enough.

5.8. Wound healing assay

Cells were seeded in 24-well plates to form confluent monolayers. The cell surface was scratched using a 10 μL pipet tip, and then cultured in fresh medium containing 1% FBS and different concentrations of agents. Bright field images of the randomly selected views along the scraped line were taken at 24 h post-scratch.

5.9. Xenograft study

Athymic BALB/c 4−6 weeks old nude mice were purchased from Hunan slike jingda experimental animal company and were housed in a specific pathogen-free room with a 12 h light/dark cycle at 25 ± 1 °C. All animal experiments were performed according to the institutional ethical guidelines established by the ethics committee of Zhengzhou University (China). For xenografts, 1.5×10^7 cells of A431 cells were injected subcutaneously at one site of anaesthetized mice. Once the tumors reached 100−200 mm³, mice were randomly divided into four groups. The control groups received physiology saline (0.1 mL/10 g) and the treatment groups received compound **WS-157** (10, 40 mg/kg) or gefitinib (10 mg/kg) by intragastric administration (i.g.) per day for a period of 27 days. The tumor size was measured and recorded at 2-day intervals after administration. After day 27, animals were sacrificed by cervical dislocation and the tumors were isolated and weighed, and then the tissue protein was extracted by RIPA buffer (Solarbio). Tumor size was determined by caliper measurements, and the body weight was measured at 2-day intervals to monitor drug toxicity.

5.10. Permeability assay

For transport experiments, Caco-2 cells (passage 35) were seeded at approximately 6.5×10^4 cells/cm² on polycarbonate 24-well Transwells® (Corning Costar Corporation, Cambridge, MA, USA) (3.0 μmol/L mean pore size). 0.5 mL of culture medium with cells was seeded to the apical (AP) side and 1.5 mL of blank culture medium was added to the basolateral (BL) side. And the cells were allowed to grow 21 days for transport experiments. Transepithelial electrical resistance (TEER) of the monolayers was measured using the Millicell-ERS system (Millipore Corp., Bedford, MA, USA) before and after the drug transport experiments. The TEER values of Caco-2 monolayers were all >400 Ω/cm². We used metoprolol, atenolol and erythromycin as a high permeable control, a low permeable control and an efflux substrate, respectively.

The assay was conducted in HBSS solution. AP−BL transport assay: 0.8 mL of test compounds (10 μmol/L) was added to the AP side and 0.4 mL of blank HBSS was added to the BL side. BL−AP transport assay: 0.4 mL of test compounds (10 μmol/L) was added to BL side and 0.8 mL of blank HBSS was added to the AP side. The plates were shaken at 37 °C for 90 min. The concentrations of the compounds in donor and receptor sides were determined by LC−MS/MS. The apparent permeability coefficient (P_{app}) of the compounds was calculated according to the following Eq. (1):

$$P_{app} = (VA/(A \times T)) \times ([Drug]_{accepter}/([Drug]_{initial, donor})) \quad (1)$$

where VA is the volume in the acceptor well, A is the surface area of the membrane (0.7 cm²) and T is the total transport time in seconds.

5.11. Metabolic stability

Metabolic stability was evaluated in liver microsomes of five different species, including human, rat, mouse, dog and monkey.

The *in vitro* metabolic reactions were incubated in PBS buffer (pH = 7.4). 30 μL of 1.5 μmol/L **WS-157** or gefitinib and 0.75 mg/mL microsomes solution was added to a new Eppendorf tube. Then, 15 μL of NADPH stock solution (6 mmol/L) was added to the Eppendorf tube to start the reaction maintained at 37 °C. After 0, 5, 15, 30 and 45 min of incubation, the reaction was ended by adding 135 μL of acetonitrile containing internal standard (IS). The quenched samples were vortexed for 10 min and centrifuged at $4325 \times g$ for 10 min. Then, the supernatant was injected for qualitative LC–MS/MS analysis.

5.12. Pharmacokinetic study

Healthy adult Sprague−Dawley rats (200 ± 20 g) were purchased from the Shanghai SLAC Laboratory Animal Co., Ltd. (Shangsha, China) and were cared under standard conditions (12/12 h light/dark cycle, humidity of 55 ± 5%, 22 ± 2 °C) in accordance with the Guidelines for Animal Experimentation of Zhengzhou University (China) and the protocol was approved by the Animal Ethics Committee of the Institution, China.

To assess the pharmacokinetic studies and compare the bioavailability of **WS-157** and gefitinib in rat, rats ($n = 6$ for each compound) were intragastrically or intravenously administered. Approximately 150 μL of whole blood were collected in K2EDTA tube *via* tail vein under anesthesia and cardiac puncture for terminal bleeding at 0.25, 0.5, 1, 3, 6 and 24 h after intragastric administration of **WS-157** or gefitinib (40 mg/kg). Blood samples were put on ice and centrifuged at $2000 \times g$ for 5 min to obtain plasma sample within 15 min. Blood samples were collected at 0.083, 0.25, 0.5, 1, 3, 6 and 24 h after intravenous administration of **WS-157** or gefitinib (10 mg/kg) and processed similarly to the per os (*p.o.*) group. The supernatant plasma was stored at −70 °C until analysis. The rats were humanely euthanized by carbon dioxide 24 h after experiment without pain.

An aliquot of 20 μL plasma sample was added with 400 μL acetonitrile containing 100 ng/mL diclofenac (internal standard, IS). The mixture was vortexed for 10 min and centrifuged at $4325 \times g$ for 10 min. An aliquot of 5 μL supernatant was injected for qualitative LC–MS/MS analysis.

LC–MS/MS analysis of the compounds was conducted by UPLC–MS/MS-22 (Triple QuadTM 6500) by a Waters BEH C18 (50 mm × 2.1 mm, 1.7 μmol/L). The temperature of column oven was maintained at 60 °C during the separation. The mobile phase was as follows: (A) aqueous phase: 0.025% formic acid and 1 mmol/L NH_4Ac in water; (B) organic phase: 5 mmol/L NH_4Ac in methanol. The gradient elution was at a flow rate of 0.6 mL/min. Compounds were eluted in the following gradient conditions: the initial proportion was 2% B and hold for 0.4 min, and increased to 65% B in 0.3 min, further to 90% in 0.5 min and maintained for 0.6 min, followed by decreasing to 2% B within 0.01 min; the whole gradient time was 2.5 min. The mass spectrometric detection was performed with an electrospray ionization (ESI) source in positive mode. Quantification was acquired by multiple reaction monitoring (MRM) mode of m/z 419.1 → 128.1 at 1.36 min for **WS-157**, m/z 447.3 → 128.3 at 1.48 min for gefitinib and m/z 296.2 → 214.2 at 1.48 min for IS.

Acknowledgments

Appendix A.   Supporting information

References

1. Sun QM, Miao ZH, Lin LP, Gui M, Zhu CH, Xie H, et al. BB, a new EGFR inhibitor, exhibits prominent anti-angiogenesis and antitumor activities. *Cancer Biol Ther* 2014;**8**:1640−7.
2. Bublil EM, Yarden Y. The EGF receptor family: spearheading a merger of signaling and therapeutics. *Curr Opin Cell Biol* 2007;**19**:124−34.
3. Ciardiello F, Tortora G. EGFR antagonists in cancer treatment. *N Engl J Med* 2008;**358**:1160−74.
4. Normanno N, De Luca A, Bianco C, Strizzi L, Mancino M, Maiello MR, et al. Epidermal growth factor receptor (EGFR) signaling in cancer. *Gene* 2006;**366**:2−16.
5. Ishikawa T, Seto M, Banno H, Kawakita Y, Oorui M, Taniguchi T, et al. Design and synthesis of novel human epidermal growth factor receptor 2 (HER2)/epidermal growth factor receptor (EGFR) dual inhibitors bearing a pyrrolo[3,2-*d*]pyrimidine scaffold. *J Med Chem* 2011;**54**:8030−50.
6. Smaill JB, Palmer BD, Rewcastle GW, Denny WA, McNamara DJ, Dobrusin EM, et al. Tyrosine kinase inhibitors. 15.4-(Phenylamino) quinazoline and 4-(phenylamino)pyrido[*d*]pyrimidine acrylamides as irreversible inhibitors of the ATP binding site of the epidermal growth factor receptor. *J Med Chem* 1999;**42**:1803−15.
7. Wissner A, Overbeek E, Reich MF, Floyd MB, Johnson BD, Mamuya N, et al. Synthesis and structure−activity relationships of 6,7-disubstituted 4-anilinoquinoline-3-carbonitriles. The design of an orally active, irreversible inhibitor of the tyrosine kinase activity of the epidermal growth factor receptor (EGFR) and the human epidermal growth factor receptor-2 (HER-2). *J Med Chem* 2003;**46**:49−63.
8. Yang J, Wang LJ, Liu JJ, Zhong L, Zheng RL, Xu Y, et al. Structural optimization and structure−activity relationships of N^2-(4-(4-methylpiperazin-1-yl)phenyl)-N^8-phenyl-9*H*-purine-2,8-diamine derivatives, a new class of reversible kinase inhibitors targeting both EGFR-activating and resistance mutations. *J Med Chem* 2012;**55**:10685−99.
9. Barker AJ, Gibson KH, Grundy W, Godfrey AA, Barlow JJ, Healy MP, et al. Studies leading to the identification of ZD1839 (IRESSA™): an orally active, selective epidermal growth factor receptor tyrosine kinase inhibitor targeted to the treatment of cancer. *Bioorg Med Chem Lett* 2001;**11**:1911−4.
10. Moyer JD, Barbacci EG, Iwata KK, Arnold L, Boman B, Cunningham A, et al. Induction of apoptosis and cell cycle arrest by CP-358,774, an inhibitor of epidermal growth factor receptor tyrosine kinase. *Cancer Res* 1997;**57**:4838−48.
11. Tan F, Shen X, Wang D, Xie G, Zhang X, Ding L, et al. Icotinib (BPI-2009H), a novel EGFR tyrosine kinase inhibitor, displays potent efficacy in preclinical studies. *Lung Cancer* 2012;**76**:177−82.
12. Engelman JA, Janne PA. Mechanisms of acquired resistance to epidermal growth factor receptor tyrosine kinase inhibitors in non-small cell lung cancer. *Clin Cancer Res* 2008;**14**:2895−9.

13. Kobayashi S, Boggon TJ, Dayaram T, Jänne PA, Kocher O, Meyerson M, et al. *EGFR* mutation and resistance of non-small-cell lung cancer to gefitinib. *N Engl J Med* 2005;**352**:786−92.

14. Minkovsky N, Berezov A. BIBW-2992, a dual receptor tyrosine kinase inhibitor for the treatment of solid tumors. *Curr Opin Investig Drugs* 2008;**9**:1336−46.

15. Solca F, Dahl G, Zoephel A, Bader G, Sanderson M, Klein C, et al. Target binding properties and cellular activity of afatinib (BIBW 2992), an irreversible ErbB family blocker. *J Pharmacol Exp Ther* 2012;**343**:342−50.

16. Food and Drug Administration. Public Health Service, U.S. Department of Health and Human Services. Shared risk evaluation mitigation strategy for all immediate-release transmucosal fentanyl dosage forms. *J Pain Palliat Care Pharmacother* 2012;**26**:123−6.

17. Sequist LV, Soria JC, Goldman JW, Wakelee HA, Gadgeel SM, Varga A, et al. Rociletinib in *EGFR*-mutated non-small-cell lung cancer. *N Engl J Med* 2015;**372**:1700−9.

18. Li ZR, Suo FZ, Hu B, Guo YJ, Fu DJ, Yu B, et al. Identification of osimertinib (AZD9291) as a lysine specific demethylase 1 inhibitor. *Bioorg Chem* 2019;**84**:164−9.

19. Greig SL. Osimertinib: first global approval. *Drugs* 2016;**76**:263−73.

20. Zhang X, Peng T, Ji X, Li J, Tong L, Li Z, et al. Design, synthesis and biological evaluation of novel 4-anilinoquinazolines with C-6 urea-linked side chains as inhibitors of the epidermal growth factor receptor. *Bioorg Med Chem* 2013;**21**:7988−98.

21. Deng X, Okram B, Ding Q, Zhang J, Choi Y, Adrián FJ, et al. Expanding the diversity of allosteric Bcr-Abl inhibitors. *J Med Chem* 2010;**53**:6934−46.

22. He PX, Zhang J, Che YS, He QJ, Chen Y, Ding J. G226, a new epi-polythiodioxopiperazine derivative, triggers DNA damage and apoptosis in human cancer cells *in vitro via* ROS generation. *Acta Pharmacol Sin* 2014;**35**:1546−55.

23. He PX, Che YS, He QJ, Chen Y, Ding J. G226, a novel epi-polythiodioxopiperazine derivative, induces autophagy and caspase-dependent apoptosis in human breast cancer cells *in vitro*. *Acta Pharmacol Sin* 2014;**35**:1055−64.

24. Zhang J, Wang Y, Shen Y, He P, Ding J, Chen Y. G9a stimulates CRC growth by inducing p53 Lys373 dimethylation-dependent activation of *Plk1*. *Theranostics* 2018;**8**:2884−95.

25. Citri A, Yarden Y. EGF-ERBB signalling: towards the systems level. *Nat Rev Mol Cell Biol* 2006;**7**:505−16.

26. Walgren RA, Walle T. The influence of plasma binding on absorption/exsorption in the Caco-2 model of human intestinal absorption. *J Pharm Pharmacol* 1999;**51**:1037−40.

27. Li Z, Ding L, Li Z, Wang Z, Suo F, Shen D, et al. Development of the triazole-fused pyrimidine derivatives as highly potent and reversible inhibitors of histone lysine specific demethylase 1 (LSD1/KDM1A). *Acta Pharm Sin B* 2019;**9**:794−808.

28. Wang S, Zhao L, Shi XJ, Ding L, Yang L, Wang ZZ, et al. Development of highly potent, selective, and cellular active tri-azolo[1,5-*a*]pyrimidine-based inhibitors targeting the DCN1−UBC12 protein−protein interaction. *J Med Chem* 2019;**62**:2772−97.

29. Yuan S, Yu B, Liu HM. Brønsted acid-catalyzed direct C (*sp²*)-H heteroarylation enabling the synthesis of structurally diverse biaryl derivatives. *Adv Synth Catal* 2019;**361**:59−66.

30. Blay J, Valentine-Braun KA, Northup JK, Hollenberg MD. Epidermal-growth-factor-stimulated phosphorylation of calpactin II in membrane vesicles shed from cultured A-431 cells. *Biochem J* 1989;**259**:577−83.

31. Hegedüs C, Truta-Feles K, Antalffy G, Várady G, Német K, Özvegy-Laczka C, et al. Interaction of the EGFR inhibitors gefitinib, vande-tanib, pelitinib and neratinib with the ABCG2 multidrug transporter: implications for the emergence and reversal of cancer drug resistance. *Biochem Pharmacol* 2012;**84**:260−7.

32. Leggas M, Panetta JC, Zhuang Y, Schuetz JD, Johnston B, Bai F, et al. Gefitinib modulates the function of multiple ATP-binding cassette transporters *in vivo*. *Cancer Res* 2006;**66**:4802−7.

33. Chang L, Xiao M, Yang L, Wang S, Wang SQ, Bender A, et al. Discovery of a non-toxic [1,2,4]triazolo[1,5-*a*]pyrimidin-7-one (WS-10) that modulates ABCB1-mediated multidrug resistance (MDR). *Bioorg Med Chem* 2018;**26**:5006−17.

34. Huang L, Fu L. Mechanisms of resistance to EGFR tyrosine kinase inhibitors. *Acta Pharm Sin B* 2015;**5**:390−401.

35. Zhang Z, Guo X, To K, Chen Z, Fang X, Luo M, et al. Olmutinib (HM61713) reversed multidrug resistance by inhibiting the activity of ATP-binding cassette subfamily G member 2 *in vitro* and *in vivo*. *Acta Pharm Sin B* 2018;**8**:563−74.